Physical parameterization in MRI

ALEXEY PROTOPOPOV
Radiology – Medical Physics
University Medical Center Freiburg
79106 Freiburg, Breisacher Str. 60a
GERMANY
proto.alex@hotmail.com , alexey.protopopov@uniklinik-freiburg.de

Abstract: – Gradient recalled echo (GRE) sequences are nowadays routinely used in clinical applications of magnetic resonance imaging (MRI). Contrast of GRE images is determined by several different physical mechanisms, like proton density, T_2 relaxation time, gradients of magnetic field, and spatial heterogeneities of spin-spin interaction. Although the combined effect of all these parameters is of great value for physicians, it is possible that their separate mapping may reveal new features, that are masked in traditional GRE images. Separate mapping of physical parameters, contributing to contrast of GRE images, is called the parameterization, and has not been entirely solved by now. The present publication reports on development of the necessary tools for the solution. Finally, results obtained on volunteers are presented.

Key-Words: - Gradient recalled echo (GRE); relaxation function; least squares; magnetic gradients.

Received: July 3, 2017. Revised: December 18, 2017. Accepted: January 26, 2018. Published: February 3, 2018

1 Introduction

A common parameter used to describe the rate of spin-spin relaxation in the presence of local magnetic field gradients is the T_2^* time, which is calculated by fitting a monoexponent over the relaxation curve. While nowadays parameter T_2^* is commonly considered to be an evolution of the T_2 decay time (first described in [1]), its original purpose was to describe the width of the relaxation spectrum [2], and the parameter itself was not directly related to relaxation speed. However, subsequent theoretical research showed that the behavior of spin-spin relaxation is more complex than a monoexponent, and structural characteristics of biological tissues are encoded in the shape of relaxation curve rather than in a single parameter T_2^* [3-9]. Furthermore, the difference between the shape of a monoexponential curve and the relaxation curve affected by local magnetic field gradients and T_2 heterogeneities meant that T_2^* is a surrogate without any significant physical meaning. Several attempts have been made to introduce a more accurate relaxation model [10, 11], but none of them were able to provide an example of how well the new model fits the experimental data. The present report introduces the concept of physical parameterization in MRI based on analysis of a shape of relaxation curves. As three Cartesian coordinates x, y, z determine position of the voxel in the body, the shape of the relaxation curve may be considered as the 4th coordinate that determines its structure. Based on the tissue model, it is possible to define the unique relaxation curve shape in each voxel with various numerical parameters, which characterize the tissue structure.

2 Problem Formulation

For practical implementation of the concept of the 4th coordinate, the four basic components are needed:

- analytical 3D model of relaxation process;
- non-iterative multi-point algorithm with clamping (MPC) for determining the analytical form of relaxation function;
- approximation function, valid for the entire time range: from zero to infinity;
- branching algorithm of spatial averaging of relaxation signals;
- resolution-preserving composite colour imaging (RPCC).

3 Problem Solution

The work on a 3D relaxation model, first presented in [12] and later expanded in [13], gives the following formula for gradient recalled echo (GRE) signal:

$$S(t) = S_0 \cdot e^{-t/T_2+\beta t^2} \cdot R_{p_x}(\alpha_x t) \cdot R_{p_y}(\alpha_y t) \cdot R_{p_z}(\alpha_y t), \quad (1)$$

where function $R(t)$ accounts for all possible gradients:

$$R_p(x) = \frac{1}{x}\int_0^x \cos(pu)e^{-u^2}\,du\,. \qquad (2)$$

Here $\alpha_{x,y,z}$ and $p_{x,y,z}$ are the coefficients describing the magnetic field gradients, and β is the coefficient responsible for the T_2 heterogeneities. By applying a Taylor expansion to approximate (1) at low t, we can turn the formula into

$$S(t) = S_0 \cdot \exp\left[-t/T_2 + \left(\beta^2 - \alpha^2\right)t^2\right], \qquad (3)$$

which can be fitted to a curve non-iteratively with the help of the least squares condition. Due to the use of a Taylor expansion, this method works only at low t, so the experimental points are assigned dynamic statistical weights based on their distance from the start of the time coordinate, so that only the appropriate points are used in the fitting. This method is named «Multiple Point Algorithm with Clamping» or MPC.

In order to calculate parameters such as $T_{1/e}$, which is the time it takes for the signal to decrease by a factor of e, one would need an approximation function that provides an adequate fit across the entire range of t: from zero to infinity. This Full Range Approximation (FRA) would also need to be analytical, since it will need to be calculated for each individual pixel of the image. Furthermore, the function in question would need to have physical meaning and not contradict reality. Finally, it must not contradict the polynomial exponent used for fitting in [12] around zero, as well as pass through the first and last points of the experimental curve. The main purpose of this last condition is to make the approximation easier to compute. The following function fulfils all of these requirements:

$$S(t) \approx \exp\left[a - bt - w\left(e^{-\varepsilon t} - 1 + \varepsilon t\right)\right]. \qquad (4)$$

Parameters a, b and c are provided by the MPC algorithm, while w and ε are derived from them in order to match the function with the experimental curve.

Due to its non-linear nature, this system is best solved using an iterative method. At the first step, we take the last experimental point at t_m and assume that $\varepsilon t_m \gg 1$ and $e^{-\varepsilon t_m} \approx 0$, which produces

$$\varepsilon^{(0)} = \frac{2ct_m}{y_m - bt_m - a}\,. \qquad (5)$$

This value is not precise enough to be used for plotting the curve, but it can be used to produce the first set of parameters using the following general formula:

$$\begin{cases} w^{(n+1)} = \dfrac{-z_m}{e^{-\varepsilon^{(n)}t_m} - 1 + \varepsilon^{(n)}t_m}; \\ \varepsilon^{(n+1)} = \sqrt{\dfrac{-2c}{w^{(n+1)}}}, \end{cases} \qquad (6)$$

where n is the number of the current iteration. This operation can be repeated an unlimited number of times, however the number of iterations typically stays below 10 in practice. Fig.1 shows an example of the full-range approximation being fitted over an experimental curve.

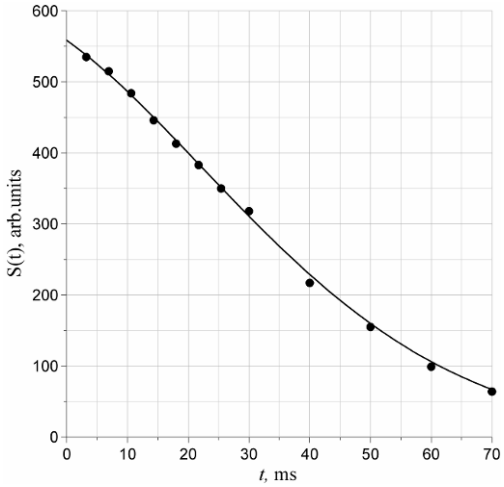

Fig.1. Solid line – FRA, points – experimental data.

The methods described above require the signal-to-noise ratio (SNR) to be above a certain value. Specifically, the MPC algorithm produces reliable results only at SNR > 60. While this is achievable with sequences of sufficiently long duration, many patient related applications do not allow such luxury. For example, due to significant displacement of internal organs during the breathing cycle, imaging of the abdominal region must often be with the patient holding breath, which limits the duration of the sequence to ~20 seconds. In other words, the signal quality required for MPC may not always be provided by the sequence. This can be rectified by introducing a branching method of spatial averaging. The difference between a standard spatial averaging algorithm and an averaging algorithm with branching is simple: the former uses

the same area around the central pixel for each echo time, while the latter dynamically adjusts the area depending on the amplitude of the signal – assuming that the level of noise would be the same for each echo, a stronger signal would have a better SNR and would therefore require a smaller averaging area. This way, the averaging area seems to branch out as illustrated on Fig.2, which gives this algorithm its name.

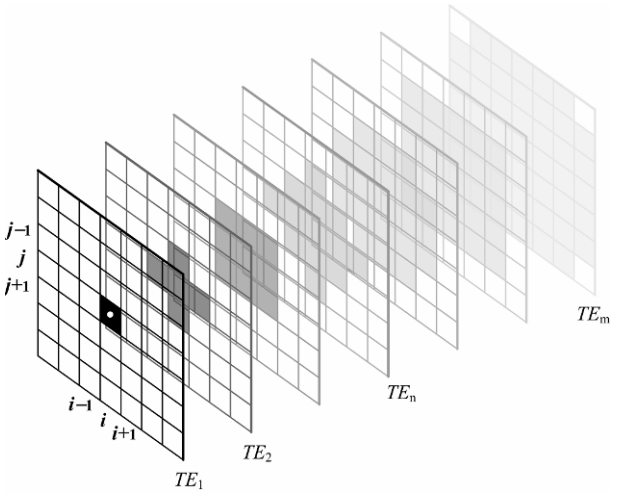

Fig.2. Concept of branching averaging. Pixels used for the averaging calculation are shown in black. The decrease in signal amplitude with subsequent TEs is depicted by the opacity of each layer of the image.

In addition to branching, adjustment of statistical weights of the pixels used in averaging was implemented in this work. The weight of the central pixel would be set by the operator in the range between one and zero, and the weights of all surrounding pixels would be adjusted automatically. For example, with the averaging area encompassing four pixels arranged around a central pixel, the statistic weights of the pixels would need to comply with the following equation:

$$4\beta + \alpha = 1, \tag{7}$$

where α is the weight of the central pixel, and β is the individual weight of every surrounding pixel. This way, if $\alpha = 1$, all pixels but the central one are ignored, and no averaging is performed. Conversely, with $\alpha = 0.2$, all pixels have the same statistic weight.

Yet despite the implementation of the branching, this averaging algorithm reduces the resolution of the calculated parameter map. To offset that, the Resolution Preserving Colour Compounds (RPCC) were used. The concept of this method is simple. The intensity of a colour pixel is typically split between three channels: red, green and blue. It can be presented as

$$\vec{P}_{i,j} = 256\left(r_{i,j} \quad g_{i,j} \quad b_{i,j}\right), \tag{8}$$

where *i* and *j* are the coordinates, the parameters *r*, *g* and *b* vary between zero and one, and 256 i s the maximum commonly used brightness value. MRI images are generally presented as grayscale images, which have the same intensity in all three channels:

$$\vec{P}_{i,j} = a_{i,j}\left(1 \quad 1 \quad 1\right) \tag{9}$$

What the RPCC does, is take the value of the parameter map $u_{i,j}$, and substitute it into one of the channels of the original MRI image, while the data from the original image is substituted into another channel:

$$\vec{P}_{i,j} = a_{i,j}\left(1 \quad u_{i,j}/u_{\max} \quad 1\right), \tag{10}$$

where $u_{\max}$ is the maximum value across the entire parameter map. This way, the parameter map is displayed as a variation of colour, while at the same time maintaining the resolution of the original MRI image. Thus, the RPCC allows the use of spatial averaging to calculate the parameter map without sacrificing the resolution of the image.

A method similar to the one presented in thisarticle was described in [14]. However, there the original image and the parameter map were assigned to separate channels:

$$\vec{P}_{i,j} = \left(a_{i,j} \quad u_{i,j} \quad 0\right) \tag{11}$$

4 Results

The sequence used for the experiments performed in this article was a standard Siemens gradient recalled echo sequence (GRE). Twelve separate echoes were acquired with each sequence, with echo times ranging between 2.6 ms and 70 ms. Scans of the head were taken using a standard birdcage coil, while the abdomen and hips were imaged using a standard flexible body coil. Fig.3 shows the results. It is immediately apparent, that the T_2 and $T_{0.5}$. For example, the liver in the abdominal images is darker than the surrounding tissues on the $T_{0.5}$ map, while on the T_2 map it is brighter. Furthermore, the

gradient colourmap noticeably highlights the borders between different organs, where changes in susceptibilities between different organs create magnetic field gradients.

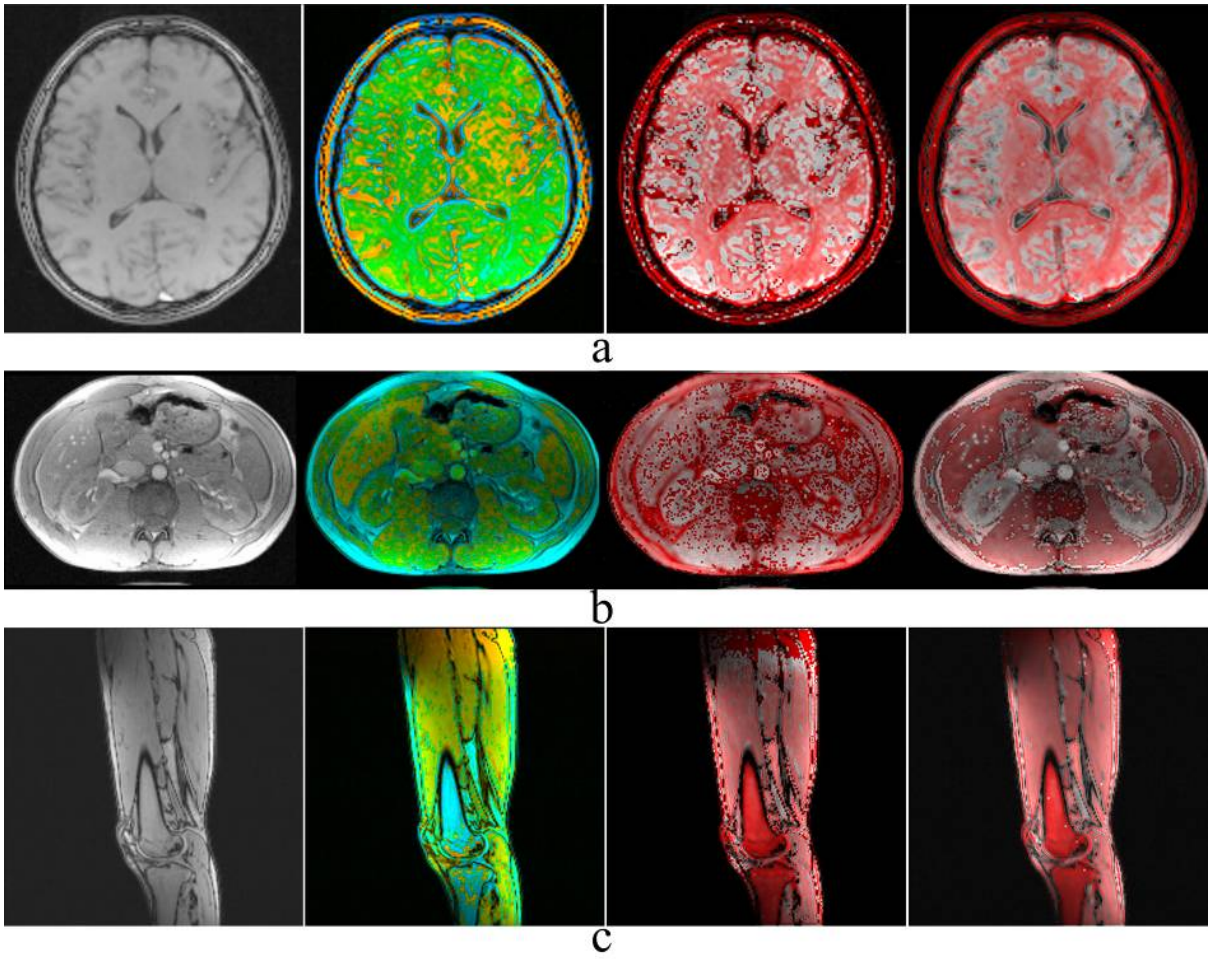

Fig.3. The rows of colour images correspond to: (a) brain, (b) abdomen, (c) hip. In each row, the first image is the original GRE image, followed by the maps of T_2, $T_{0.5}$ and, finally, a colourmap of gradients created using RPCC.

5 Discussion

The concept of the 4th dimension splits every original GRE image into a series of maps, showing spatial distribution of physically meaningful parameters, like T_2, average gradients, $T_{0.5}$, or others. Thus, from pure intensity rendering in conventional GRE imaging, we come to mapping of physical parameters relevant to specific clinical applications, such as BOLD. In addition, the gradient map reveals many details not present in the original image. It is also important to note, that all of these maps were acquired using a si ngle sequence. On one hand, this means a reduction in time required for the scan, since the GRE sequence can be considered one of the faster sequences used in MRI. On the other hand, this also reduces the overall exposure of the patient to RF radiation. Both of these qualities are valuable when the subject needs to undergo a long examination involving many sequences. Finally, while this article presents T_2, $T_{0.5}$ and gradient maps as results, many more parameters can be derived from the shape of the relaxation curve, including, but not limited to total volume under the curve, decay rate and spin density. It is entirely possible, that with further study one could establish a correlation between these parameters and various pathological conditions.

Acknowledgement

The author is grateful to Prof. M. Bock for support and encouragement.

References:

[1] Bloch, F., Nuclear induction, *Phys. Rev.*, Vol.70, No.7-8, 1946, pp. 460–474.

[2] Bloembergen, N., Purcell, E.M., Pound, R.V., Relaxation effects in nuclear magnetic resonance absorption, *Phys. Rev.,* Vol.73, No.7, 1948, pp. 679–712.

[3] Yablonskiy, D.A, Haacke, E.M., Theory of NMR signal behavior in magnetically inhomogeneous tissues – the static dephasing regime, *Magn. Reson. Med.*, Vol.32, No.6, 1994, pp. 749–763.

[4] Sukstanskii, A.L, Yablonskiy, D.A., Gaussian approximation in the theory of MR signal formation in the presence of structure-specific magnetic field inhomogeneities, *Journ. Magn. Res.*, Vol.163, 2003, pp. 236–247.

[5] Sukstanskii, A.L, Yablonskiy, D.A., Gaussian approximation in the theory of MR signal formation in the presence of structure-specific magnetic field inhomogeneities. Effects of impermeable susceptibility inclusions, *Journ. Magn. Res.*, Vol.167, 2004, pp. 56–67.

[6] Kiselev, V.G., Effect of magnetic field gradients induced by microvasculature on NMR measurements of molecular self-diffusion in biological tissues, *Journ. Magn. Res.*, Vol.170, 2004, pp. 228–235.

[7] Dickson, J.D, Ash, T.W.J, Williams, G.B., Sukstanskii, A.L, Ansorge, R.E, Yablonskiy, D A., Quantitative phenomenological model of the BOLD contrast mechanism, *Journ. Magn. Res.*, Vol.212, 2011, pp. 17–25.

[8] Knight, M.J, Kauppinen, R.A., Diffusion-mediated nuclear spin phase decoherence in cylindrically porous materials, *Journ. Magn. Res.*, Vol.269, 2016, pp. 1–12.

[9] Wharton, S, Bowtell, R., Fiber orientation-dependent white matter contrast in gradient echo MRI, *Proc. National Acad. Sci. USA*, 2012 Vol.109, 2012, pp. 18559–18564. Supporting information 10.1073/pnas.1211075109.

[10] Fernandez-Seara, M.A, Wehrli, F.W., Postprocessing technique to correct for background gradients in image-based R2* measurements, *Magn. Reson. Med.*, Vol.44, 2000, pp. 358–366.

[11] Dahnke, H, Schaeffter, T., Limits of detection of SPIO at 3.0T using T_2^* relaxometry, *Magn. Reson. Med.*, Vol.53, 2005, pp. 1202–1206.

[12] Protopopov, A., Relaxation model and mapping of magnetic field gradients in MRI, *Appl. Magn. Reson.*, Vol.48, No.3, 2017, pp. 255-274.

[13] Protopopov, A., Structural analysis of relaxation curves in MRI, *Appl. Magn. Reson.*, Vol.48, No.8, 2017, pp. 783-794.

[14] Valdés Hernández, M.C., Royle, N.A., Jackson, M.R., et al., Color fusion of magnetic resonance images improves intracranial volume measurement in studies of aging, *Open Journal of Radiology*, Vol.2, 2012, pp. 1–9.